


Identification of Phase Inversion on Sieve Trays

Jonas Schulz, Philipp Aziz, and Hans-Jörg Bart*

DOI: 10.1002/cite.202000140

 This is an open access article under the terms of the Creative Commons Attribution License, which permits use, distribution and reproduction in any medium, provided the original work is properly cited.

The fundamental differences in hydrodynamics of the froth and spray regime account for the ongoing interest in search for the point of phase inversion. This short communication presents a new approach for identification of phase inversion on sieve trays in terms of an image-based measurement technique. Image analysis of entrained droplets reveals a distinct increase in Sauter mean diameter and droplet frequency during phase inversion. Further measurement methods like pressure drop, gravimetric analysis of entrained liquid, froth height assessment and photographic observation of the flow regime serve as a reference value and complement the discussion. A flow map based on the experimental data comprises each regime and shows a good agreement with phase inversion correlations from literature.

Keywords: Droplet size distribution, Entrainment, Image analysis, Phase inversion, Transition regime

Received: July 14, 2020; *revised:* October 19, 2020; *accepted:* November 10, 2020

1 Introduction

The identification of phase inversion on sieve trays is of considerable interest concerning the amount of entrained liquid, which distinctly increases at operation in the spray regime [1]. Particularly, vacuum distillation comes along with excessive entrainment rates favored by low weir loads [2, 3]. Nevertheless, column operation far off the spray regime in a weakly developed froth or even bubble regime is unpreferred as well due to decreasing liquid mixing and interfacial area [3]. Since the 1950s, research to identify the transition from froth to spray regime is ongoing [4–7]. As given correlations significantly differ in their prediction of the transition regime, this article intends to assess the phase inversion with different measurement techniques. Conventional tray pressure drop and weighing of entrained liquid from the column head are combined with image analysis of the froth height and droplet regime. In addition, the photographic capture of the operating column enables a visual evaluation of the flow regime present on the tray.

2 Theoretical Background

Common two-phase regimes on sieve trays are froth, spray, emulsion, bubble and cellular foam, while the latter two possess less industrial relevance. Liquid on the tray penetrated by single bubbles represents a common bubble regime, which usually occurs close to tray weeping. High liquid loads at low gas loads favor an emulsion regime containing small bubbles emulsified by the high velocity of the liquid flowing over the tray. Trays operating in the froth regime show a continuous liquid phase with a dispersed gas phase in form of bubbles, while the spray regime features a dispersed liquid phase in form of droplets surrounded by a

continuous gas phase [2]. The phase inversion or so-called transition regime marks off froth and spray and entails characteristics of both regimes [8]. As spray and froth are fundamentally different it remains difficult to describe both with one model [6, 9]. Spray regimes preferably develop in case of high gas loads and low liquid loads [10], which are often present at low-pressure or vacuum distillation [2, 3]. Trays loaded with high to moderate liquid flow rates and moderate to low gas flow rates predominantly form a froth regime [11]. By now, different measurement methods are applied in order to identify the phase inversion on sieve trays. Assessment of density profiles along the column height with gamma-ray absorption techniques represents an approach of observing the transition regime by distinct changes of the dispersion density [3, 12] but also requires a sophisticated effort [6]. Deployment of a light technique that records changes in transmitted light intensity during column operation at a specific height above the tray is successfully applied by Payne and Prince [13], while Pinczewski and Fell [14] doubt of the validity of this method due to a less clear difference between the light intensities of froth and spray regime. Their counterproposal comprises an electrical resistance probe installed inside a single sieve hole, which indicates the phase inversion to spray by a strong decline in the electrical resistance due to jetting in the sieve hole [14]. Determination of entrainment rates by a capture tray with weighing of the entrained liquid volume [12] or by conductivity methods [15] represents an alternative apart from examinations at the regime itself.

Jonas Schulz, Philipp Aziz, Prof. Dipl.-Ing. Dr. techn. Hans-Jörg Bart

bart@mv.uni-kl.de

Technische Universität Kaiserslautern, Chair of Separation Science and Technology, Gottlieb-Daimler-Straße 44, 67663 Kaiserslautern, Germany.

Additionally, pressure drop measurements constitute an attempt to track regime changes by pressure changes of the gas phase [6, 12]. Further, visual judgements of the regime present on the tray are encountered as a double check to the aforementioned methods [6, 14].

By now, detection and analysis of entrained droplets above the regime with image-based measurement techniques is solely performed with regards to entrainment analysis [16, 17] but not for identification of the phase inversion. Thereby, this article applies an image-based measurement technique to identify the phase inversion from froth to spray by changes in the respective droplet size distributions (DSD). Besides conventional measurement methods like entrainment rate quantification by weighing and pressure drop measurements, the analysis of droplet regime and froth height enable a direct observation of the two-phase layer and its reaction to operation changes of the column. Several correlations are available for identification of the transition regime. As the gas load is expected to be immanent for column operation [6], this study aims to identify the transition regime in terms of a critical F-factor. The F-factor describes the gas velocity on the tray bubbling area multiplied by the square root of the gas density [18]. Jeronimo and Sawistowski [4] provide a correlation for identification of the phase inversion by considering the liquid load besides several tray design parameters and fluid properties. Eq. (1) describes the relation:

$$v_{g,h,t} = \frac{0.655 \left(\frac{g(\rho_l - \rho_g)\sigma^2}{d_h \rho_g^3} \right)^{0.167}}{\varphi \left(1 + 0.000104 \frac{\dot{L}}{l_w} \varphi^{-0.59} \right) \varphi^{-1.79}} \quad (1)$$

The hole gas velocity $v_{g,h,t}$ at the transition is described by surface tension σ , hole diameter d_h , the ratio of hole to bubbling area φ , liquid flow across the tray \dot{L} , outlet weir length l_w and the liquid and gas densities ρ_l and ρ_g . Pinczewski and Fell [5] provide a correlation, which estimates the superficial gas velocity at phase inversion $v_{g,t}$ (Eq. (2)):

$$v_{g,t} = \frac{2.75 \left(\frac{\dot{L}}{l_w} \sqrt{\rho_l} \right)^{0.91 \frac{d_h}{\varphi}}}{\sqrt{\rho_g}} \quad (2)$$

Both correlations are derived from experiments of Pinczewski and Fell [14] in a single-stage test rig with different single-pass rectangular trays ($A_b = 0.182 \text{ m}^2$, $d_h = 0.0064\text{--}0.0191 \text{ m}$, \dot{L}/l_w up to $58 \text{ m}^3 \text{ m}^{-1} \text{ h}^{-1}$). Lockett [7] considers the clear liquid height $h_{c,t}$ at phase inversion in order to estimate the occurrence of the transition regime, as given in Eq. (3):

$$v_{g,h,t} = \frac{h_{c,t}}{2.78 d_h \sqrt{\frac{\rho_g}{\rho_l}}} \quad (3)$$

The correlation is derived from experiments in a three-stage test rig ($d_{co} = 0.46 \text{ m}$) with different single-pass trays ($A_b = 0.104 \text{ m}^2$, $d_h = 0.0032\text{--}0.0127 \text{ m}$, $\dot{L}/l_w \approx 2\text{--}24 \text{ m}^3 \text{ m}^{-1} \text{ h}^{-1}$). The clear liquid height $h_{c,t}$ at phase inversion is predicted with the correlation of Hofhuis and Zuiderweg [3]. Each equation is convertible to the aforementioned critical F-factor at the transition F_t ($v_{g,h,t} A_b / A_{co} = v_{g,t} \rightarrow v_{g,t} A_{co} / A_b \rho_g^{0.5} = F_t$).

3 Material and Methods

3.1 Test Rig

The test rig relevant for this contribution is a glass column ($d_{co} = 0.457 \text{ m}$) equipped with a capture tray (Raschig GmbH) and a measurement section (RVT Process Equipment GmbH) for insertion of the aforementioned image-based measurement technique. Measurements are performed at a height of 0.343 m above the last tray. The column is equipped with two sieve trays ($d_h = 0.011 \text{ m}$; $A_b = 0.139 \text{ m}^2$; $\varphi = 5.7 \%$). The height of the inlet weir is adjusted to 0.05 m , while the outlet weir height h_w is set to the same height. The length of the outlet weir comes up to $l_w = 0.24 \text{ m}$. A centrifugal pump delivers water from the column bottom to the last sieve tray, while a high-pressure blower delivers unsaturated air to the column bottom. The gas enters the column vertically and centered to the column axis in order to enable a homogenous gas distribution. Already low gas and liquid loads acquire high humidity levels above the last tray. Each experiment is conducted at room temperature ($\approx 293 \text{ K}$) and ambient pressure ($\approx 1 \text{ bar}$). Further details on the test rig including a detailed outline are delineated in [19]. Tab. 1 summarizes the operating points relevant for this contribution.

As phase inversion carries a great weight for vacuum distillation due to excessive entrainment in the spray regime, this communication confines on low weir loads following recommendations of Hoppe and Mittelstrass [20] and Stichlmair [21] and the aforementioned test rigs of Lockett et al. [15] and Pinczewski and Fell [14].

3.2 Measurement Techniques

Several measurement techniques are applied for assessment of the phase inversion. At first, wet and dry pressure drop per sieve tray are determined with aid of a differential pressure cell (Ahlborn Mess- und Regelungstechnik GmbH; FDA602S6K). Image-based measurements of the droplet regime are acquired by the modified optical multimode online probe (OMOP), which captures images of the entrained droplets rich in contrast with aid of an area camera (Basler AG; ace series), telecentric illumination in transmitted light and a telecentric lens (Edmund Optics CompactTL™ series). Further information on the modified

Table 1. Operating points examined in scope of this contribution.

| Liquid flow per m weir length [m ³ m ⁻¹ h ⁻¹] | Liquid flow per column cross sectional area [m ³ m ⁻² h ⁻¹] | Superficial gas velocity based on column cross sectional area [m s ⁻¹] | F-factor based on bubbling area [Pa ^{0.5}] |
|--|--|---|---|
| 1.25 | 1.8 | 0.93 | 1.2 |
| 2.5 | 3.7 | 1.1 | 1.4 |
| 3.75 | 5.5 | 1.24 | 1.6 |
| 5 | 7.3 | 1.4 | 1.8 |
| 6.25 | 9.1 | 1.54 | 2 |
| 7.5 | 11 | 1.7 | 2.2 |
| 10 | 14.6 | 1.85 | 2.4 |

OMOP including a detailed outline are given in [19]. Image analysis of footage from a single-lens reflex camera (Nikon K.K.; D5600) equipped with a zoom lens (Sigma K.K.; f/3.5–6.3) enable a determination of the froth height above the last sieve tray and serve as documentation for the visual inspection of the regime. Assessment of the entrainment rate by weighing of the entrained liquid volume is acquired by the aforementioned capture tray (Raschig GmbH). Fig. 1 presents an outline of the test rig including the discussed measurement techniques.

3.3 Methodological Approach

Independent of the measurement technique, the test rig starts up for 30 min with the intent to acquire a steady state, thus a reliable starting situation for the subsequent experiments, which are executed with 15 min idle time between each measuring point. Each measuring point consists of 7500 images captured by the modified OMOP, 10 photographic images captured by the reflex camera, 1 min recording of differential pressure at 10 Hz and at least five samples of weighed entrainment with the requirement to weigh at

least three equal rates in a series. Recording of dry and wet pressure drop according to Pinczewski et al. [12] enables a detailed analysis of the hydraulic behavior of the tray. Image analysis of the droplet regime is conducted with ImageJ [22], which includes binarization by the Otsu algorithm [23], background subtraction in case of nonuniform image illumination and median filter to remove image inequalities caused by impurities on the camera sensor. Further information on the image analysis procedures applied by the modified OMOP are delineated in [19, 24–27]. The integration of a calibration scale in each photographic image enables a simple metering of the froth height with ImageJ at several positions (min. 4, max. 59) over the column width depending on the local contrast ratio within the froth.

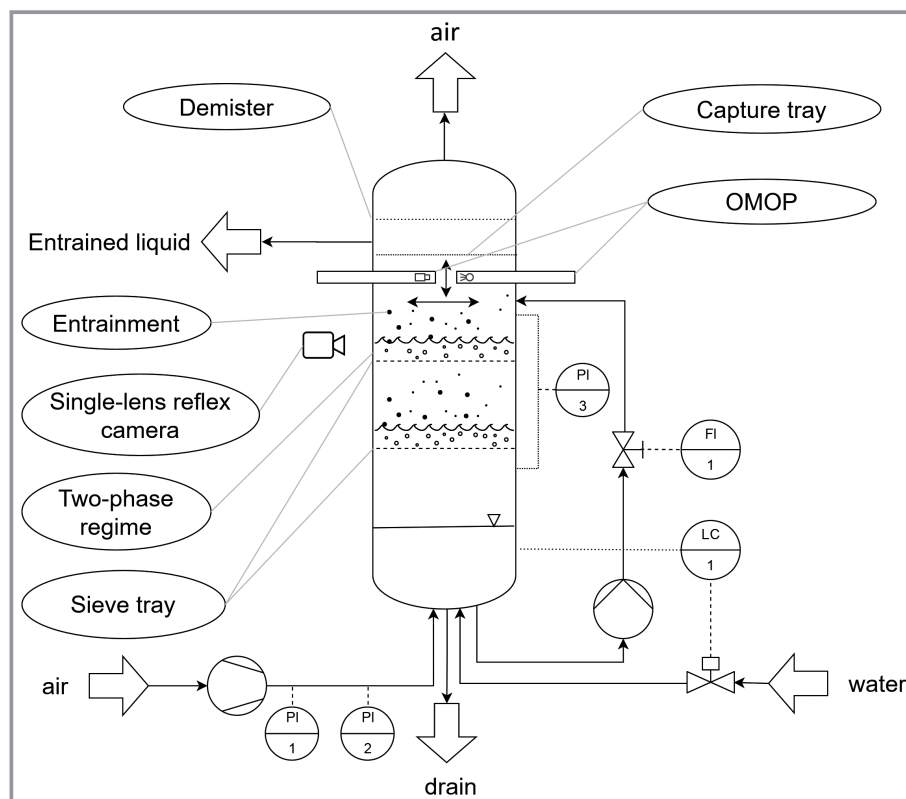


Figure 1. Test rig including modified OMOP, single-lens reflex camera, capture tray with demister and differential pressure cell (PI 3).

4 Experimental Results

The graphs of Fig. 2 depict measurements of dry Δp_{dr} and wet Δp_{we} pressure drop over F-factor at several weir loads. The left ordinate refers to wet pressure drop ($\Delta p_{we} = \Delta p_{tot} - \Delta p_{dr}$), while the right ordinate depicts dry pressure drop. At first dry pressure drop ($0 \text{ m}^3 \text{ m}^{-1} \text{ h}^{-1}$) is compared to the correlation of Pinczewski et al. [12], which represents a minor modification of the early pressure drop correlation of Hunt et al. [28]. In order to obtain a better data fit, the variable constant C is changed to a value of 1.0 compared to 1.3 applied by Pinczewski et al. [12].

The wet pressure drop measurements show a slight decline between the low F-factors 0.6 to $1.0 \text{ Pa}^{0.5}$, which is increasing at higher weir loads. It is expected that this progression originates from a hindrance of the very slow gas phase to pass the liquid layer resting on the tray. Most likely, the regime changes from bubbling to froth. Another trend is apparent at low liquid loads of 1.25 – $2.5 \text{ m}^3 \text{ m}^{-1} \text{ h}^{-1}$ and the F-factor of $1.6 \text{ Pa}^{0.5}$, where the wet pressure drop shows a local maximum. Pinczewski et al. [12] are not capable of identifying a maximum in wet and dry pressure drop progression. Still, they find a small maximum in the difference of dry and wet pressure drop, which they interpret as the point of phase inversion [12]. Payne and Prince [29] conduct a slightly refined pressure drop measurement in terms of a subtraction of dry and hydrostatic pressure from total pressure drop. This so-called residual pressure drop has a maximum during phase inversion, as the passage of the gas inside the orifice changes from bubbling to jetting. They are capable of showing this maximum in a batch apparatus containing a single orifice plate without liquid cross-flow [29]. Further experiments in an expanded test rig with liquid crossflow and sieve plates instead of a single-orifice plate show difficulties in reproducing this maximum. Trays with high fractional hole areas and operation in liquid crossflow tend to show a continuous increase of residual pressure drop instead of a maximum [13]. For this measuring points, Payne and Prince [13] substitute the residual pressure drop by the transmitted light intensity technique. As mentioned before, Pinczewski and Fell [14] criticize the use of this method for trays with liquid cross flow due to a less clear difference between the light intensities of

froth and spray regime. As residual pressure drop measurements require an enhanced installation effort, rather impractical for industrial plants, the measurement of wet and dry pressure drop is favored here. As can be seen in Fig. 2, weir loads higher than $3.75 \text{ m}^3 \text{ m}^{-1} \text{ h}^{-1}$ show just a smaller gradient instead of a local maximum at the same F-factor of $1.6 \text{ Pa}^{0.5}$, although shifting the phase inversion and by that the local maximum to higher gas loads is expected. Thereby, the here reported pressure drops are capable of indicating regime changes from bubbling over froth to spray. Still, they do not pose a reliable measure for identification of the phase inversion. Measurements of entrainment rate by weighing the entrained liquid collected by a capture tray and assessment of froth height by image analysis are depicted in Fig. 3.

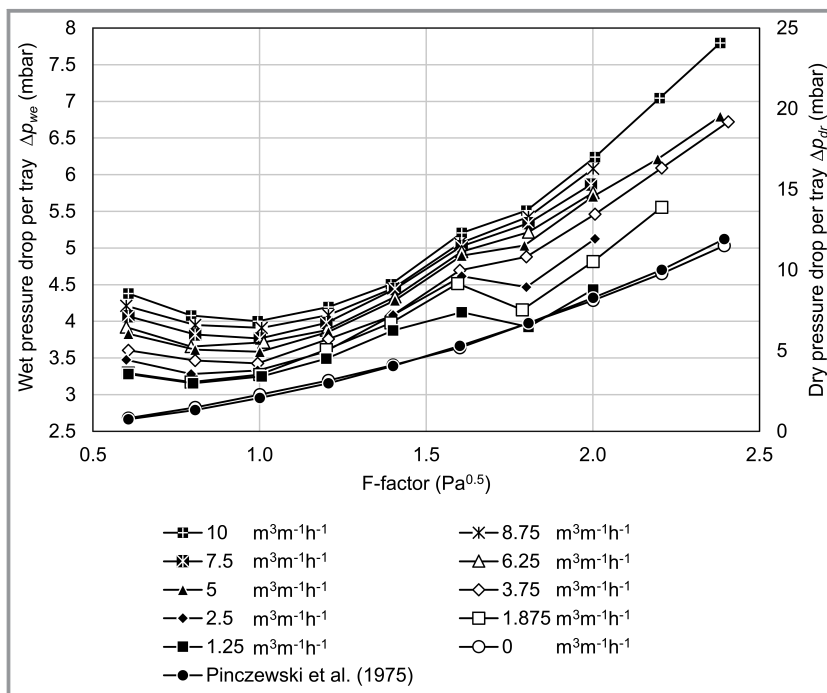


Figure 2. Dry Δp_{dr} and wet Δp_{we} pressure drop over F-factor at different weir loads.

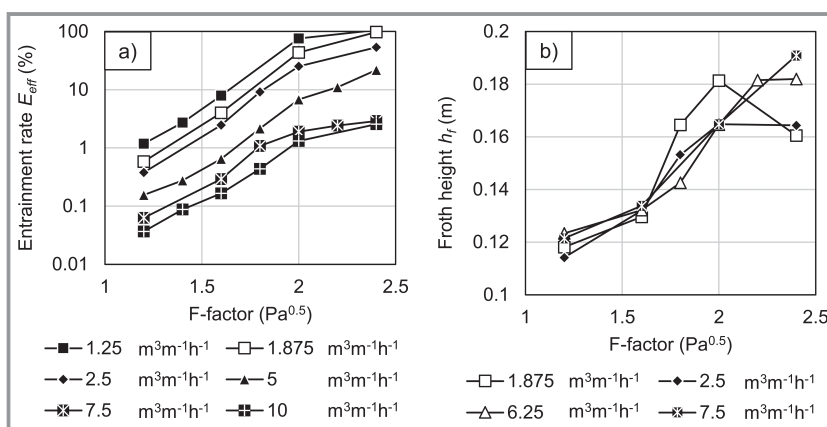


Figure 3. a) Entrainment rate and b) froth height over F-factor at different weir loads.

With respect to Fig. 3a, most weir loads show a smaller incline at low gas loads, followed by a sharper increase in entrainment, which often recedes at higher F-factors and low weir loads due to incoming dry blowing. This behavior corresponds to the findings of other contributions, which expect a distinct increase in entrainment at phase inversion moving the tray from the froth towards the spray regime [1, 3, 12, 15, 30]. For example, the weir load of $5 \text{ m}^3 \text{ m}^{-1} \text{ h}^{-1}$ shows the steepest increase in entrainment between F-factors 1.6 and $2 \text{ Pa}^{0.5}$ indicating an entrance from froth to transition regime. Fig. 3b presents detected froth heights for several weir loads. Here again, a sharp incline in froth height is recognizable for liquid loads $1.875 \text{ m}^3 \text{ m}^{-1} \text{ h}^{-1}$ ($1.6\text{--}1.8 \text{ Pa}^{0.5}$) and $6.25 \text{ m}^3 \text{ m}^{-1} \text{ h}^{-1}$ ($1.8\text{--}2 \text{ Pa}^{0.5}$). In addition, froth height declines at F-factor $2.4 \text{ Pa}^{0.5}$ with respect to $1.875 \text{ m}^3 \text{ m}^{-1} \text{ h}^{-1}$ and stagnates at $2.4 \text{ Pa}^{0.5}$ with respect to weir load of $6.25 \text{ m}^3 \text{ m}^{-1} \text{ h}^{-1}$. Visual observation finds that dry blowing and a well-established spray regime are the regimes behind this trend. Nevertheless, the progression of entrainment rates and froth heights rather provide indications on phase inversion similar to the pressure drop measurements. Dry blowing clearly becomes apparent through a declining increase of entrainment rates and collapsing froth heights due to the inconstant liquid flow on the tray. Figs. 4a and 4b depict Sauter mean diameter d_{32} and frequency f_d of entrained droplets at several weir loads acquired by the modified OMOP.

The progression of the Sauter mean diameter reveals an effect already shown in Fig. 3b. With respect to the weir load of $1.875 \text{ m}^3 \text{ m}^{-1} \text{ h}^{-1}$, the droplet size and froth height rapidly increase between a F-factor of $1.6 \text{ Pa}^{0.5}$ and $1.8 \text{ Pa}^{0.5}$ due to phase inversion from froth to transition regime. The droplet size now slightly declines (Fig. 4a; F-factor $1.8\text{--}2.0 \text{ Pa}^{0.5}$), which originates from a stronger atomization of droplets due to an enhanced spray regime. Also, Banerjee et al. [31], who use an impingement method (MgO) for assessment of the droplet size, show a declining increase of Sauter mean diameters at the point of phase inversion. A further increase of the gas load to $2.4 \text{ Pa}^{0.5}$ moves the tray from a very intense spray regime towards dry blowing. The harsh decline in froth height (Fig. 3b) and the excessive entrainment rate (Fig. 3a) of nearly 100% confirm a dry blowing very clearly. In Fig. 3b, one can observe an unstable operation condition of dry blowing, which enables a froth height determination as the liquid discontinuously bottles up on the tray followed up by a complete entrainment

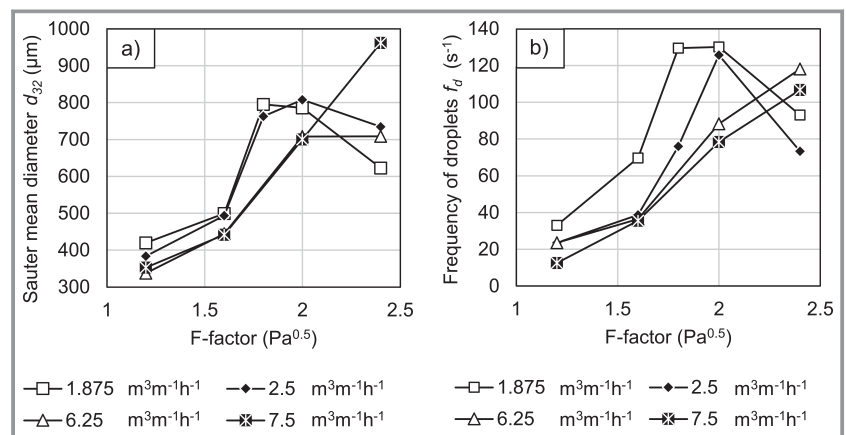


Figure 4. a) Sauter mean diameter d_{32} and b) droplet frequency f_d over F-factor at different weir loads.

of the liquid phase. Fig. 5 illustrates the behavior of the flow regime at the weir load of $1.875 \text{ m}^3 \text{ m}^{-1} \text{ h}^{-1}$ acquired by the photographic observation, which serves as a basis for the visual inspection.

The next higher weir load of $2.5 \text{ m}^3 \text{ m}^{-1} \text{ h}^{-1}$ shows a similar progression, which is again confirmed by entrainment rate and froth height (see Fig. 3). The higher weir loads of 6.25 and $7.5 \text{ m}^3 \text{ m}^{-1} \text{ h}^{-1}$ show a weakening of the increase in Sauter mean diameter. Droplet sizes distinctly increase at higher gas loads and do not shrink at high F-factors. For instance, the weir load of $6.25 \text{ m}^3 \text{ m}^{-1} \text{ h}^{-1}$ shows a first strong reduction in the increase of Sauter mean diameter from F-factor 2.0 to $2.4 \text{ Pa}^{0.5}$, due to phase inversion to spray regime. The liquid load of $7.5 \text{ m}^3 \text{ m}^{-1} \text{ h}^{-1}$ shows a linear increase in Sauter mean diameter, which underlines an even later phase inversion to spray from F-factor $2.4 \text{ Pa}^{0.5}$. The droplet frequency depicted in Fig. 4b properly highlights the behavior of the two-phase regime under increasing gas loads. The increasing gas velocity generates more and more droplets. At a specific velocity, the gas penetrates the sieve hole in form of a gaseous jet instead of single bubbles [14]. The gas jet now entrains a far larger number of droplets, which start to decrease in size if the velocity is further increased [29]. Higher liquid loads decrease the number of generated droplets and shift the phase inversion to higher

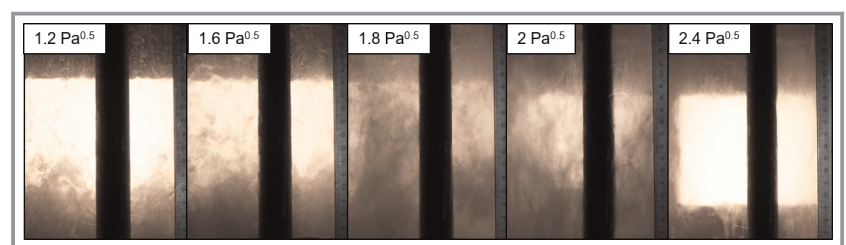


Figure 5. Photographic observation of flow regimes (weir load $1.875 \text{ m}^3 \text{ m}^{-1} \text{ h}^{-1}$) with froth ($1.2 \text{ Pa}^{0.5}$), phase inversion ($1.6\text{--}1.8 \text{ Pa}^{0.5}$), spray ($1.8\text{--}2 \text{ Pa}^{0.5}$) and dry blowing ($2.4 \text{ Pa}^{0.5}$).

gas loads [15, 16]. In this sense, the image analysis concentrates on identification of the highest gradients with respect to Sauter mean diameter and droplet frequency in order to identify the transition regime. The analysis reveals a mean incline of the Sauter mean diameter of 52 % (min. 33 %, max. 59 %) and a mean incline of the droplet frequency of 102 % (min. 55 %, max. 176 %) at phase transition over all studied weir loads. To put this more simply, at phase transition mean droplet size grows by a half, while droplet frequency in average doubles. Furthermore, it is noteworthy that the image analysis acquired by the modified OMOP finds a Sauter mean diameter between 700 and 800 μm at the transition regime for each studied weir load. Of course, this droplet size depends on the used sieve tray ($d_h = 0.011\text{ m}$; $A_b = 0.139\text{ m}^2$; $\varphi = 5.7\%$) and the measurement height of 0.343 m and will vary with changes in inlet design and installation height of the probe. Nevertheless, Banerjee et al. [31] find similar droplet sizes of roughly 875 μm at a hole size of 0.008 m and a measurement height of 0.2 m during phase inversion. The results of the image analysis, photographic observations and entrainment rate assessment enable a summary in form of a flow map. Tab. 2 comprises the assessment criteria and selectivity of each measurement method for the required regime identification.

With respect to the change from bubble to froth regime, each measurement method is marked with N/A, as the belonging experiments run at F-factors above $1.0\text{ Pa}^{0.5}$, except for wet pressure

drop and visual judgment. Regarding the Sauter mean diameter d_{32} and droplet frequency f_d , a stagnation in terms of a missing considerable change from phase inversion to a fully developed spray regime is expected, as enhanced gas velocities result in a stronger atomization of droplets and counteract a further distinct increase in size or frequency. Throughout each run, the visual inspection of the regime remains very useful for the regime identification and the evaluation of the other methods. Fig. 6 depicts the aforementioned flow map. In addition, the phase inversion correlations of Lockett [7], Pinczewski and Fell [5] as well as Jeronimo and Sawistowski [4] are integrated for comparison with the experimental data.

The transition regime outlined in the flow map shows a good agreement with the phase inversion prediction of

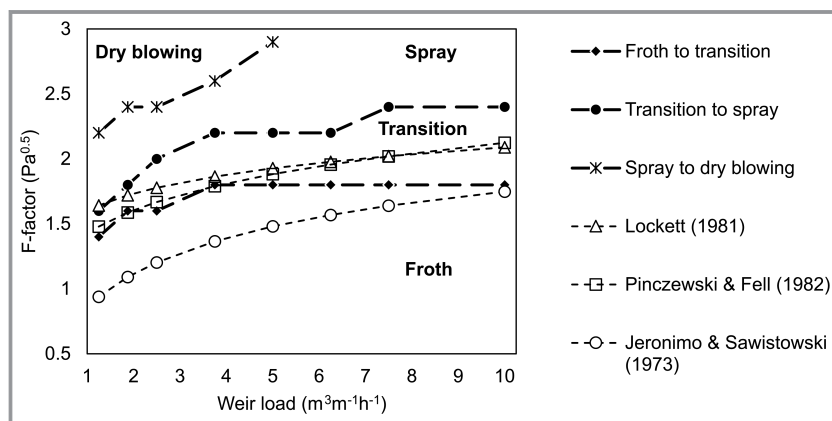


Figure 6. Flow map for sieve tray ($d_h = 0.011\text{ m}$; $A_b = 0.139\text{ m}^2$; $\varphi = 5.7\%$) including froth, spray and transition regime plus undesired operation phenomenon dry blowing.

Table 2. Assessment criteria and selectivity of each measurement method for regime identification (++ very high, + high, 0 moderate, - low).

| Measurement method | Bubble \rightarrow Froth | | Froth \rightarrow Transition | | Transition \rightarrow Spray | | Spray \rightarrow Dry blowing | |
|--------------------|--|-------------|---|-------------|---|-------------|--|-------------|
| | Assessment criterion | Selectivity | Assessment criterion | Selectivity | Assessment criterion | Selectivity | Assessment criterion | Selectivity |
| Δp_{we} | Minimum | + | Local maximum | - | N/A | | N/A | |
| E_{eff} | N/A | | Distinct increase | 0 | Distinct increase | 0 | Stagnation at excessive value | ++ |
| h_f | N/A | | Steep increase | + | Declining increase | 0 | Steep decrease | + |
| d_{32} | N/A | | Distinct increase | ++ | Stagnation or declining increase | + | Distinct decrease | + |
| f_d | N/A | | Steep increase | ++ | Stagnation or declining increase | + | Distinct decrease | + |
| Visual inspection | Distinct uprising bubbles in continuous liquid phase | ++ | Torn open froth surface with intensified droplet generation | ++ | Turbulent froth layer and height plus high droplet generation | ++ | Excessive hole jetting up to fully dry trays (discontinuous operation) | + |

Pinczewski and Fell [5] and Lockett [7], whereas the constant 2.78 is changed to 2.05 in Eq. (3). Here, the phase inversion correlation of Jeronimo and Sawistowski [4] underestimates the gas load in terms of the F-factor required for a regime change from froth to spray.

5 Conclusion and Outlook

The presented work applies several measurement methods for identification of transition between froth and spray regime. Droplet size distribution and froth height acquired by image analysis together with visual inspection of the regime documented by photographic footage represent the most promising techniques for regime identification, due to proximity to the two-phase layer. Indirect measurements like pressure drop or entrainment rate rather provide indications on regime changes. In this sense, it is expected that optical measurement methods represent a feasible approach to identify phase inversion [3, 6, 13, 31]. Image analysis reveals a distinct increase of Sauter mean diameter and droplet frequency at the phase transition. The applied image-based system is also capable of analyzing droplet regimes under higher weir loads [17] or in larger column diameters, which enables additional research. Specifically, the identification of phase inversion on large trays suffering of maldistribution represents an interesting issue for further studies.

We wish to thank the German Federal Ministry for Economic Affairs and Energy for their financial support and our partners in the joint project TERESA (Tropfenentstehung und Reduzierung in Stoffaustauschapparaten; FKZ 03ET1395H; teresa-projekt.de). Open access funding enabled and organized by Projekt DEAL.

Symbols used

| | | |
|------------|-----------------------------------|---------------------------------------|
| A | [m ²] | Area |
| d | [m] | Diameter |
| E_{eff} | [%] | Entrainment rate based on liquid load |
| f | [s ⁻¹] | Frequency |
| F | [Pa ^{0.5}] | F-factor |
| g | [m s ⁻²] | Gravitational acceleration |
| h | [m] | Height |
| l | [m] | Length |
| \dot{L} | [m ³ s ⁻¹] | Liquid flow rate |
| Δp | [mbar] | Differential pressure |

Greek symbols

| | | |
|--------|-----------------------|----------|
| v | [m s ⁻¹] | Velocity |
| ρ | [kg m ⁻³] | Density |

| | | |
|-----------|-----------------------|----------------------------|
| σ | [kg s ⁻²] | Surface tension |
| φ | [-] | Hole / bubbling area ratio |

Abbreviations

| | |
|------|--------------------------------|
| DSD | Droplet Size Distribution |
| fps | Frames per second |
| OMOP | Optical Multimode Online Probe |

Subscripts

| | |
|-------|-------------------|
| b | Bubbling area |
| c | Clear liquid |
| co | Column |
| d | Droplet |
| dr | Dry |
| f | Froth |
| g | Gas |
| h | Hole |
| l | Liquid |
| t | Transition regime |
| tot | Total |
| w | Weir |
| we | Wet |

References

- [1] M. A. Jeronimo, H. Sawistowski, *Inst. Chem. Eng. Symp. Ser.* **1979**, 56 (2), 41–56.
- [2] H. Z. Kister, *Distillation design*, McGraw-Hill, New York **2013**.
- [3] P. A. M. Hofhuis, F. J. Zuiderweg, *Inst. Chem. Eng. Symp. Ser.* **1979**, 56 (2), 2.2/1–2.2/26.
- [4] M. A. Jeronimo, H. Sawistowski, *Trans. Inst. Chem. Eng.* **1973**, 51, 265–266.
- [5] W. V. Pinczewski, C. J. D. Fell, *Ind. Eng. Chem. Proc. Des. Dev.* **1982**, 21 (4), 774–776. DOI: <https://doi.org/10.1021/i200019a038>
- [6] R. G. H. Prince, A. P. Jones, R. J. Panic, *Inst. Chem. Eng. Symp. Ser.* **1979**, 56 (2), 2.2/27–2.2/39.
- [7] M. J. Lockett, *Trans. Inst. Chem. Eng.* **1981**, 59, 26–34.
- [8] H. Z. Kister, J. R. Haas, *Ind. Eng. Chem. Res.* **1988**, 27 (12), 2331–2341. DOI: <https://doi.org/10.1021/ie00084a018>
- [9] H. Z. Kister, J. R. Haas, *Inst. Chem. Eng. Symp. Ser.* **1988**, 104, A483–A494.
- [10] P. Hofhuis, *Flow regimes on sieve trays for gas/liquid contacting*, Dissertation, Technische Hogeschool Delft **1980**.
- [11] H. Z. Kister, *Distillation operation*, McGraw Hill, New York **1990**.
- [12] W. V. Pinczewski, N. D. Benke, C. J. D. Fell, *AIChE J.* **1975**, 21 (6), 1210–1213. DOI: <https://doi.org/10.1002/aic.690210625>
- [13] G. J. Payne, R. G. H. Prince, *Trans. Inst. Chem. Eng.* **1977**, 55, 266–273.
- [14] W. V. Pinczewski, C. J. D. Fell, *Trans. Inst. Chem. Eng.* **1972**, 50, 102–108.
- [15] M. J. Lockett, G. T. Spiller, K. E. Porter, *Trans. Inst. Chem. Eng.* **1976**, 54, 202–204.
- [16] W. V. Pinczewski, C. J. D. Fell, *Trans. Inst. Chem. Eng.* **1977**, 55, 46–52.
- [17] J. Schulz, K. Schäfer, H.-J. Bart, *Chem. Ing. Tech.* **2019**, 104 (10), 202. DOI: <https://doi.org/10.1002/cite.201900112>

- [18] J. Stichlmair, *Grundlagen der Dimensionierung des Gas-Flüssigkeit-Kontaktapparates Bodenkolonne*, Verlag Chemie, Weinheim **1978**.
- [19] J. Schulz, H.-J. Bart, *Chem. Eng. Res. Des.* **2019**, *147*, 624–633. DOI: <https://doi.org/10.1016/j.cherd.2019.05.041>
- [20] K. Hoppe, M. Mittelstrass, *Grundlagen der Dimensionierung von Kolonnenböden*, Theodor Steinkopff Verlag, Dresden **1967**.
- [21] J. Stichlmair, *Chem. Ing. Tech.* **1978**, *50* (4), 281–284. DOI: <https://doi.org/10.1002/cite.330500408>
- [22] <http://imagej.nih.gov/ij/> (Accessed on October 15, 2020)
- [23] N. Otsu, *IEEE Trans Syst. Man, Cybern.* **1979**, *9* (1), 62–66.
- [24] M. Mickler, H.-J. Bart, *Chem. Ing. Tech.* **2013**, *85* (6), 901–906. DOI: <https://doi.org/10.1002/cite.201200139>
- [25] M. Mickler, S. Didas, M. Jaradat, M. Attarakih, H.-J. Bart, *Chem. Ing. Tech.* **2011**, *83* (3), 227–236. DOI: <https://doi.org/10.1002/cite.201000156>
- [26] M. Mickler, B. Boecker, H.-J. Bart, *Flow. Meas. Instrum.* **2013**, *30*, 81–89. DOI: <https://doi.org/10.1016/j.flowmeasinst.2013.01.004>
- [27] M. Lichti, X. Cheng, H. Stephani, H.-J. Bart, *Chem. Eng. Technol.* **2019**, *42* (2), 506–511. DOI: <https://doi.org/10.1002/ceat.201800340>
- [28] C. Hunt, D. N. Hanson, C. R. Wilke, *AIChE J.* **1955**, *1* (4), 441–451. DOI: <https://doi.org/10.1002/aic.690010410>
- [29] G. J. Payne, R. G. H. Prince, *Trans. Inst. Chem. Eng.* **1975**, *53*, 209–223.
- [30] F. J. Zuiderweg, *Chem. Eng. Sci.* **1982**, *37* (10), 1441–1464. DOI: [https://doi.org/10.1016/0009-2509\(82\)80001-8](https://doi.org/10.1016/0009-2509(82)80001-8)
- [31] T. S. Banerjee, N. K. Roy, M. N. Rao, *Indian J. Technol.* **1969**, *7* (10), 301–307.